Effectiveness of Current Controlled Voltage Source Converter Excited DFIG for Wind Farm Stabilization

K.E. Okedu[1], S.M. Muyeen[2], Rion Takahashi[1], and Junji Tamura[1]*

[1]Department of Electrical and Electronic Engineering, Kitami Institute of Technology, Japan

[2] Department of Electrical Engineering, The Petroleum Institute, Abu Dhabi, U.A.E.

E-mail: kenokedu@yahoo.com

Abstract — In this paper, stabilization methods of wind farms composed of fixed speed wind turbines (FSWTs) and variable speed wind turbines (VSWTs) are analyzed. A current controlled voltage source converter (CC-VSC) scheme for VSWT driving doubly fed induction generator (DFIG) is proposed. The proposed scheme is then compared with two other DFIG control schemes, to show the effectiveness of the proposed controller. Different types of symmetrical and unsymmetrical faults are analyzed considering wind farm recent grid codes. Though all of the schemes are able to stabilize the wind farms during transient conditions, the proposed CC-VSC scheme offers the advantage of less intricacy of controller design, better performance during grid fault, and omission of DC-link protection scheme, which can reduce the overall cost of the system. Moreover, extensive simulation analyses by using PSCAD/EMTDC are performed to determine the optimum amount of FSWT system that can be stabilized by VSWT system.

Keywords: Current controlled voltage source converter, Doubly fed induction generator (DFIG), Voltage controlled voltage source converter, SDBR, Grid fault, Wind energy.

I. Introduction

Wind energy conversion systems have quickly evolved over the last decades. This is because it is one of the extra ordinary sources of renewable energy. Therefore, efficient and reliable exploitation tools are necessary to make these installations more profitable. However, due to its

clean character and free availability the growth of wind energy has developed rapidly [1-3].

It was shown in [4], that the control strategies of the variable speed wind turbine have a major effect on the wind turbine and the electric loads, meaning whatever the kind of wind turbine, the control strategy remains a key factor [5]. In the last 15years, the use of doubly fed induction machines in modern variable speed wind turbines has increased rapidly. This development has been driven by the cost reduction as well as the low-loss generation of Insulated Gated Bipolar Transistors (IGBT) [6].

The doubly fed induction generator (DFIG) with a power converter is a common and efficient configuration to convert the mechanical power from the variable speed rotor to electrical power with constant grid frequency [1, 7]. The DFIG includes an induction generator with slip ring, a partial scale power electronic converter and a DC-link capacitor. The power electronic converter of the DFIG which encompasses a back to back AC-DC-AC voltage source converter has two main parts; grid side converter (GSC) and the rotor side converter (RSC). The GSC helps to maintain a constant DC-link voltage, and also to supply reactive power to the grid. The RSC controls the active and reactive power of the DFIG. The DFIG power converter only processes slip power, therefore it is designed in partial scale and just about 20-30% of the generator rated power [2, 8], which makes the DFIG system attractive from an economical point of view.

This paper proposes a current controlled voltage source converter (CC-VSC) for controlling a DFIG which is based on a CC-VSC developed for controlling a permanent magnet synchronous generator (PMSG) in [9]. An extensive comparative study using the proposed scheme and two other different control schemes for controlling a DFIG wind generator was carried out. The first scheme uses a voltage controlled voltage source converter (VC-VSC) based DFIG. The second scheme uses a VC-VSC based DFIG with a series dynamic braking resistor

(SDBR) connected at the stator of the DFIG. These schemes were developed to augment the fault ride through (FRT) capability of wind farms composed of variable speed wind turbines (VSWTs) and fixed speed wind turbines (FSWTs). The superiority of the proposed CC-VSC scheme to the VC-VSC and the SDBR schemes is that it can operate well without the support of DC-link protection during a grid fault. Moreover, the intricacy of the controller design can be reduced considerably in the proposed CC-VSC scheme. The two-mass drive train model was considered for all wind generators, as drive train modeling has great influence on the dynamics during a fault [10]. Simulations were carried out using PSCAD/EMTDC [11] for a three line to ground fault (severe case) in the considered model system, to observe the effectiveness of the schemes. The transient stability index of the system was also analyzed for different symmetrical and unsymmetrical fault conditions with different fault locations in the model system. Analysis was also carried out concerning the optimum ratio of power capacity between the DFIG and the IG taking the grid code into consideration.

II. Model System

A model system shown in Fig.1 [12] is considered in this study, where two wind farms are connected to the multi-machine power system. Aggregated wind farm model is considered in this analysis for fast computing. Each wind farm is composed of 1 DFIG and 3 IGs. The wind turbine modeling, parameters of the generators and the DFIGs excitation circuit including DC-link protection circuit, and the basic control concept of the DFIGs with VC-VSC have been presented in [12].

The IEEE generic turbine model and approximate mechanical-hydraulic speed governing system [13] is used for synchronous generator 1 (SG1). The IEEE “non-elastic water column without surge tank” turbine model and “PID control including pilot and servo dynamics” speed-

governing system [14] is used for synchronous generator 2 (SG2). IEEE alternator supplied rectifier excitation system (ACIA) [15] is used in the exciter model of both synchronous generators. All numerical values used in the model system in Fig. 1 are in p.u. The parameters of all generators are given in Table 1. The loads A, B and C have power values of (175MW, 20MVA), (90MW, 30MVA), and (150MW, 20MVA) respectively.

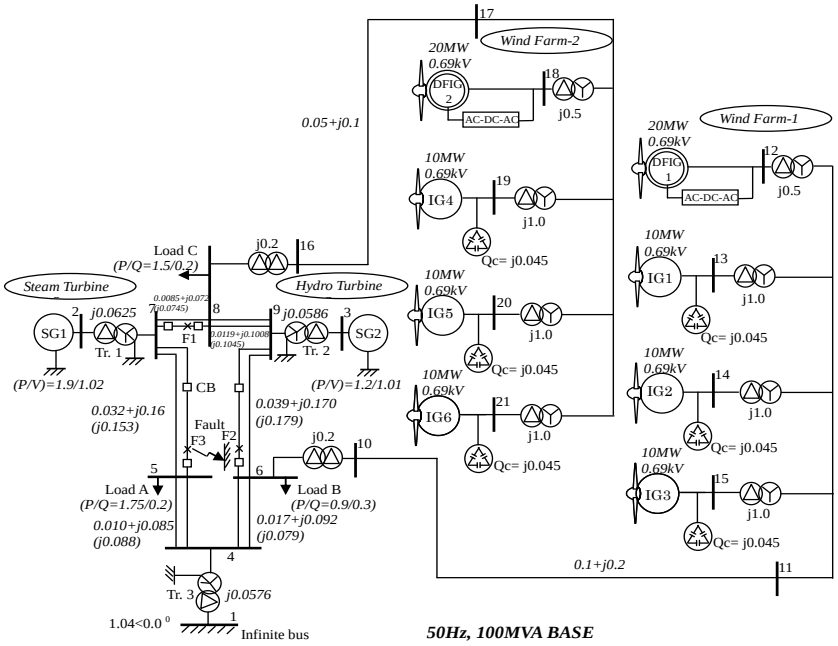

Fig. 1 Model system

Table 1: Generator Parameters

Generator Type	SG1	SG2	Generator Type	IGs	DFIGs
MVA	200	130	MVA	10	20
r_a (pu)	0.003	0.003	r1 (pu)	0.01	0.01
x_a (pu)	0.102	0.130	x1 (pu)	0.1	0.15
X_d (pu)	1.651	1.200	Xmu (pu)	3.5	3.5
X_q (pu)	1.590	0.700	r21 (pu)	0.035	0.01
X'_d (pu)	0.232	0.300	x21 (pu)	0.030	0.15
X'_q (pu)	0.380		r22 (pu)	0.014	
X''_d (pu)	0.171	0.220	x22 (pu)	0.098	
X''_q (pu)	0.171	0.250	Hg (pu)	0.3	0.3
T'_{do} (sec)	5.900	5.000	Hwt (pu)	3.0	3.0
T'_{qo} (sec)	0.535		Kw (pu)	90	90
T''_{do}(sec)	0.033	0.040			
T''_{qo}(sec)	0.078	0.050			
H (sec)	9.000	2.500			

A comparative study of fixed speed wind generator and variable speed wind generator is given in Table 2.

Table 2 Comparative study of fixed and variable speed wind generators

Fixed speed wind generator	Variable speed wind generator
1. Has fixed speed operation, thus the power captured is limited.	1. Has variable speed operation making it possible to achieve a high efficiency of energy conversion compared to constant speed operation especially in low wind speed areas.
2. Technology has limited ability to provide voltage and frequency control.	2. Ability to decouple control of active and reactive powers rapidly and independently by secondary excitation control. Thus, system tends to be more stable during network disturbances.
3. Has superior characteristics such as brushless and rugged construction, low cost, maintenance free, and operational simplicity.	3. The reduction of mechanical stresses and acoustic noise.
4. Requires large reactive power to recover the air gap flux when a short circuit fault occurs in the power system.	4. Improvement of the power quality of the system without external reactive power compensation devices.
5. The installations of reactive power compensation devices to support the fixed wind speed generators increases the overall cost of the system.	5. The required capacity of the power converters for secondary excitation can be less than half for the case of a DFIG system, and thus the total cost decreases.

Also, a comparative study of single and mult-machine system is given in Table 3.

Table 3 Comparative study of single and multi-machine system

Single machine system	Multi-machine system
1. Has only one type of machine	1. Has different types of machines
2. Simple in structure	2. Complex in structure
3. Not realistic case for study because is normally connected to an infinite bus, hence cannot be used to actually judge system performance.	3. Gives a realistic scenario of a study and can be used to effectively judge performance of a proposed system or controller.

III. DFIG Mathematical Model

A DFIG machine is a wound rotor with back-to back converter in the rotor circuit. The rotor is supplied by pulse width modulator inverter, while the stator is directly connected to the grid. The rotor current exciting frequency is controlled as the wind velocity is changed. The frequency of output power is fixed at grid frequency, which is given as

$$\omega_s = p\Omega_m \pm \omega_r \qquad (1)$$

Where ω_s is the grid electrical angular speed, Ω_m is the mechanical angular rotor speed, ω_r is the electrical angular speed of rotor variables, and p is the number of pole pairs. Eqn. (1) establishes the basis for variable speed constant frequency.

The mathematical equations of the DFIG in terms of stator, rotor voltages and flux are given as follows [16-18]:

$$V_{ds} = R_s i_{ds} - \omega_s \Phi_{qs} + \frac{d}{dt}\Phi_{ds} \quad (2)$$

$$V_{qs} = R_s i_{qs} + \omega_s \Phi_{ds} + \frac{d}{dt}\Phi_{qs} \quad (3)$$

$$V_{dr} = R_r i_{dr} - (\omega_s - \omega)\Phi_{qr} + \frac{d}{dt}\Phi_{dr} \quad (4)$$

$$V_{qr} = R_r i_{qr} + (\omega_s - \omega)\Phi_{dr} + \frac{d}{dt}\Phi_{qr} \quad (5)$$

The direct and quadrature stator and rotor flux components are given as follows [19]:

$$\Phi_{ds} = L_s i_{ds} + L_m i_{dr} \quad (6)$$

$$\Phi_{qs} = L_s i_{qs} + L_m i_{qr} \quad (7)$$

$$\Phi_{dr} = L_r i_{dr} + L_m i_{ds} \quad (8)$$

$$\Phi_{qr} = L_r i_{qr} + L_m i_{qs} \quad (9)$$

Where, V_{ds}, V_{qs}, are the d- and q-axis stator voltage, Φ_{ds}, Φ_{qs}, Φ_{dr}, Φ_{qr} are the d- and q-axis stator and rotor winding flux, i_{ds}, i_{qs}, are d- and q-axis stator current, i_{qr} and i_{dr} are d- and q-axis rotor currents (A) respectively, L_s and L_r are the stator leakage and rotor self inductances (H), and V_s is the magnitude of the stator phase voltage (V).

The d-q steady state equivalent circuit of the DFIG is shown in Fig. 2a below [20]:

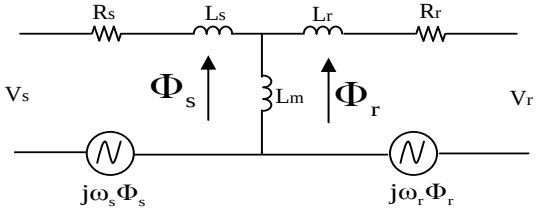

Fig. 2a Equivalent circuit of DFIG in synchronous references frame

For independent control of active and reactive power output of the DFIG, vector control is normally used. This control techniques has many advantages compared to other strategies because it makes the control algorithm simple, robust and provides fast response.

For the rotor side converter (RSC) algorithm, it is assumed that the DFIG is connected to the power grid in which the grid voltage and frequency are constant. Fixing the d-axis of the synchronous frame on the stator voltage vector, a stator voltage oriented control is obtained. The vector of the stator voltage then becomes:

$$\bar{V}_s = V_{ds} + j\,0 \qquad (10)$$

According to (10), the active power and reactive power output from the stator side of the DFIG can be represented as:

$$P_s = V_{ds} i_{ds} \qquad (11)$$

$$Q_s = -V_{ds} i_{qs} \qquad (12)$$

Putting (2) into (11) and (3) into (12) respectively, the active and reactive powers can be derived as follows:

$$P_s = \frac{V_{ds}(\Phi_{ds} - L_m i_{dr})}{L_s} \qquad (13)$$

$$Q_s = -\frac{V_{ds}(\Phi_{qs} - L_m i_{qr})}{L_s} \qquad (14)$$

From (13) and (14), the active and reactive powers of the DFIG system are related to the rotor currents i_{dr} and i_{qr} respectively. Therefore, the active and reactive power can be controlled via i_{dr} and i_{qr} respectively, which is possible through the control of V_{dr} and V_{qr}.

Fig. 2b shows the grid side converter (GSC) pulse width modulator rectifier. The aim of the control system is to maintain the DC-bus voltage to the required level for the RSC, while the

main input currents should be sinusoidal and in phase with their counterpart voltages, for which the control system of DFIG maintains unity power factor condition.

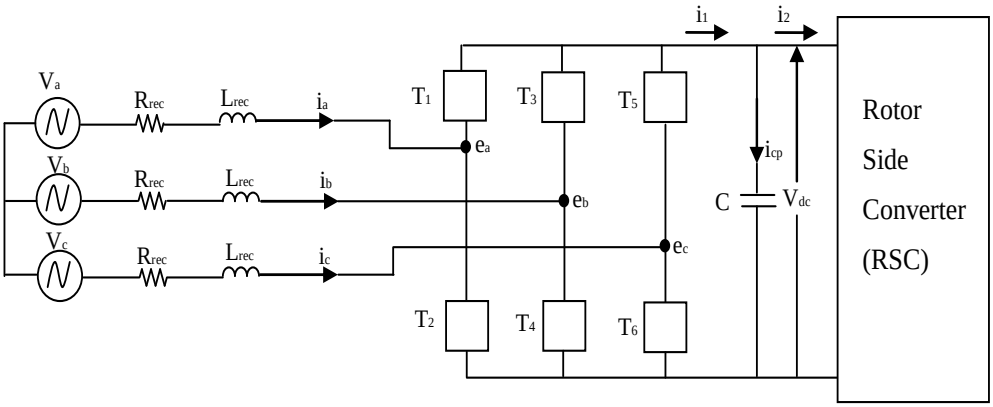

Fig. 2b Structure of the grid side converter of DFIG

For modeling and control design, the d-q synchronous frame voltage components are [16]:

$$V_d = e_d + L_{rec}\frac{d}{dt}i_d + R_{rec}i_d - \omega_s L_{rec} i_q \qquad (15)$$

$$V_q = e_q + L_{rec}\frac{d}{dt}i_q + R_{rec}i_q + \omega_s L_{rec} i_d \qquad (16)$$

Where R_{rec} and L_{rec} are resistance and inductance of boost inductor respectively.

This strategy leads to getting the following active and reactive powers:

$$P_{rec} = V_d i_d \qquad (17)$$

$$Q_{rec} = - V_d i_q \qquad (18)$$

Thus, the current command q-axis controls the reactive power, whereas a current command of d-axis controls the active power, and consequently controls indirectly the DC-link voltage.

IV. Voltage Controlled Voltage Source Converter Scheme for DFIG (Scheme 1)

The block diagram for the voltage controlled voltage source converter (VC-VSC) based DFIG which is referred as Scheme 1 is shown in Fig. 3 for the rotor and grid side converters. The control method for the DFIG is described in the following subsections for the rotor and the grid side converters.

A. Rotor side converter control

In normal operation (when the grid voltage $V_g > 0.9$), the rotor side converter (RSC) regulates the output power (P_{DFIG}) and delivers/absorbs reactive power as well. In Fig. 3, θ_{PLL} is the angle of the phase lock loop (PLL), and θ_r is the effective angle for the abc-to-dq0/dq0-to-abc transformations. The rotor side converter controls the terminal (grid) voltage to 1.0pu. The d-axis current corresponds to the active power, while the q-axis current corresponds to the reactive power. After a dq0-to-abc transformation, V_{dr}^* and V_{qr}^* are sent to the PWM signal generator. Thus, $^*Vr_{abc}$ is generated as a three-phase voltage reference for the rotor side converter, and then used for the IGBTs switching as shown in Fig. 3.

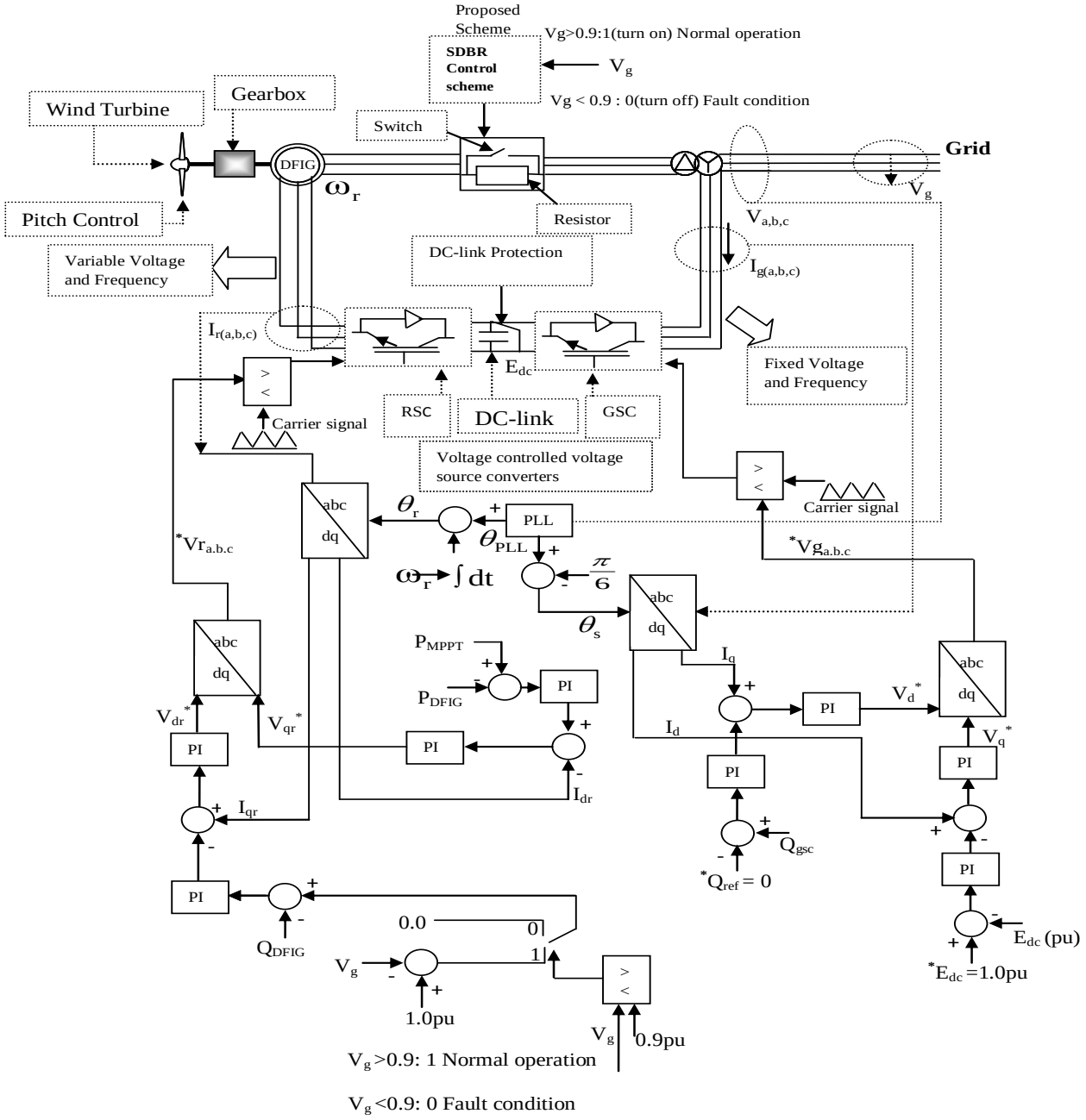

Fig. 3 Overall control system of DFIG with VC-VSC and SDBR (Schemes 1 and 2)

B. Grid side converter control

Fig. 3 also shows the control block for the grid side converter (GSC), where PLL provides the angle θ_{PLL} and θ_s is the effective angle for the abc-to-dq0/dq0-to-abc transformations. The GSC regulates the DC-link voltage (E_{dc}) to 1.0pu. The d-axis current corresponds to the DC-link

voltage, while the q-axis current corresponds to the reactive power output from the grid side converter. After a dq0-to-abc transformation, V_q^* and V_d^* are sent to the PWM signal generator. Finally ${}^*Vg_{abc}$ is generated as a three phase voltage reference for the GSC.

In light of the DFIG mathematical model presented in section III, the block diagram in Fig. 3 can be summarized mathematically as:

For rotor side converter control
$$\begin{aligned} P_{DFIG} &\alpha I_{dr} \alpha V_{qr} \\ Q_{DFIG} &\alpha I_{qr} \alpha V_{dr} \end{aligned} \quad (19)$$

For the grid side converter control
$$\begin{aligned} E_{dc} &\alpha I_d \alpha V_q \\ Q_{gsc} &\alpha I_q \alpha V_d \end{aligned} \quad (20)$$

V. Voltage Controlled Voltage Source Converter Strategy for DFIG with SDBR Considered (Scheme 2)

The control block of the DFIG rotor side converter (RSC), the grid-side converter (GSC), and the SDBR control system is shown in Fig. 3.

A scheme with a small value (0.05pu) of series dynamic braking resistor (SDBR) connected to the stator of the DFIG (Fig. 3), and the DC-link protection circuit in the rotor circuit is proposed as Scheme 2 [21, 22]. This combination can improve further the overall performance of the DFIG during a grid fault. In normal operation, the switch of SDBR is on and the resistor is bypassed, but the switch is off and the resistor is inserted into the stator circuit during a fault condition.

The difference between the SDBR and the crowbar or DC-link chopper with braking resistor is their topology. The latter is shunt–connected and can control the voltage, while the SDBR can control the stator current. Also, in the SDBR strategy, high voltage can be shared by the resistance because of the series topology. Therefore, the induced overvoltage may not lead to the loss of converter control. The SDBR not only control the rotor overvoltage which could

cause the RSC to lose control, but limits high rotor current more significantly [23]. In addition, the charging current to the DC-link capacitor can be reduced due to the rotor current limitation, and hence DC-link overvoltage, which could damage the DFIG power converter, can also be controlled. Furthermore, the SDBR can increase the generator output and hence reduce its speed increase during a voltage dip due to a grid fault [24], which can improve the post fault recovery and hence the transient stability of the DFIG system.

The SDBR starts to operate by inserting a resistor in the stator of the DFIG during a fault, and then the terminal voltage of the generator increases, resulting in increase of the electrical torque and output power. The schematic arrangement and control strategy are shown in Fig. 3. Either a bypass switch or a circuit breaker could be used for the SDBR control. But the cost of a bypass switch is less expensive than that of a circuit breaker. The bypass switch for the SDBR is normally on, but when voltage dip below 0.9pu occurs due to a grid fault, it opens to allow current to pass through a small series resistance. Current then begins to flow through the inserted resistor. When voltage is recovered above a certain specified level, the bypass switch closes and then the stator circuit restores to its normal state. During the short insertion period, the energy is dissipated in the resistor, resulting in its temperature increase. The resistor should be selected according to its temperature limit and the maximum energy which can be dissipated during the short period.

VI. Current Controlled Voltage Source Converter Strategy for DFIG System (Scheme 3)

The control block of proposed current controlled voltage source converter (CC-VSC) scheme is shown in Fig. 4, which is referred as Scheme 3. The command signals for the RSC and GSC are also shown in Fig. 4. The control system of the RSC and the GSC for the proposed CC-VSC

scheme are described in the following subsections.

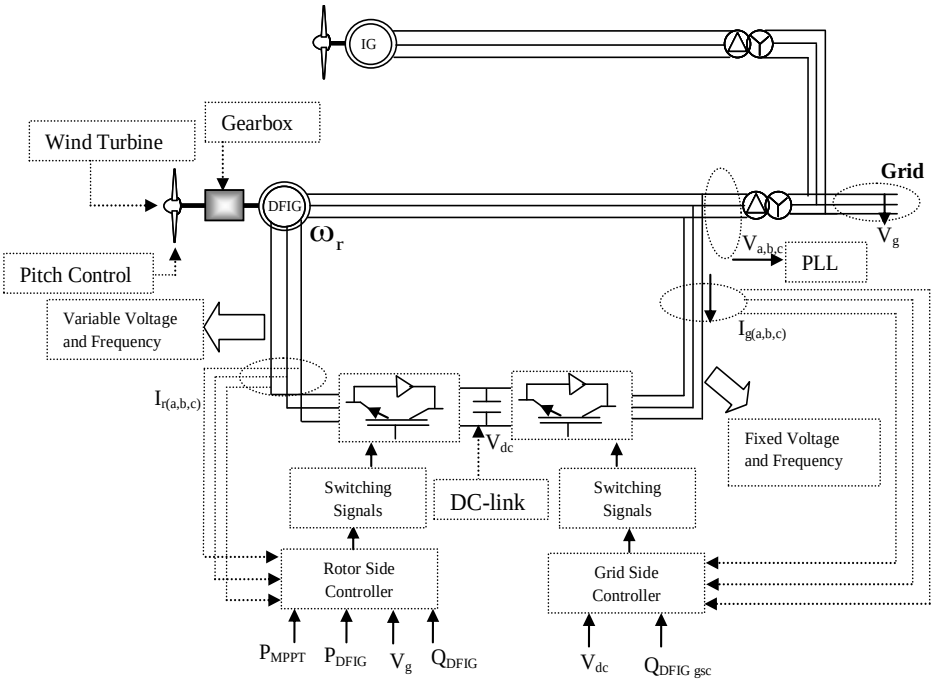

Fig. 4 DFIG with current controlled voltage source converters

A. Rotor Side Converter Control

In the rotor side converter (RSC) control shown in Fig. 5, the maximum power point tracking, P_{MPPT}, of the wind turbine is compared to the grid output of the DFIG, P_{DFIG}, to determine the reference signal for active power control. A comparator is used to determine the reference signal of the active and reactive power control during normal and fault conditions of the DFIG. During normal operation, when the grid voltage is above 0.9pu, the reference signal of the DFIG real power is P_{MPPT} of the wind turbine. The reference signal for the DFIG reactive power in normal operation is the difference between the grid voltage (pu) and 1.0pu. The error signals are then passed through PI controllers. When the grid voltage is less than 0.9pu during a grid fault, the comparator regulates the reference signals of the DFIG real and reactive power to zero. In this case, the wind turbine power is reduced to mitigate the overvoltage that is normally

experienced in the DC-link in the CC-VSC control strategy. The two reference signals from the controller are then converted from dq to abc using the rotor angle calculated from the phase lock loop (PLL). The reference rotor currents $*I_{rabc}$ are then passed through another PI controller before comparing them to the measured rotor currents $I_{r(abc)}$. The resultant signal is then compared with a carrier signal to generate the switching signals for IGBTs in the RSC. It should be noted that, the dq to abc transformation is only once in the CC-VSC but twice in the VC-VSC scheme. Thus the intricacies of the controller design are reduced in the CC-VSC scheme.

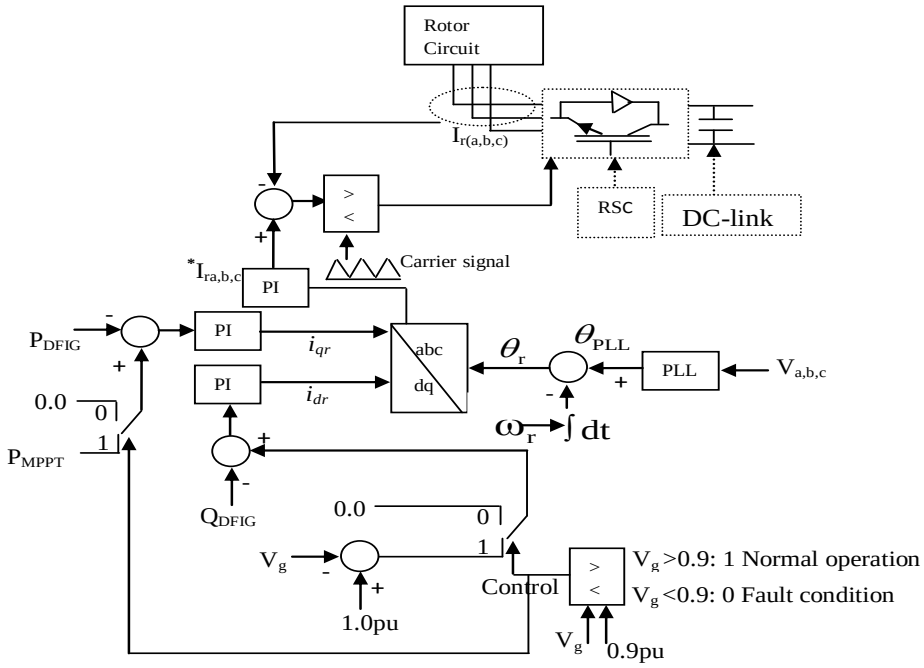

Fig. 5 Block diagram of rotor side converter control of DFIG

B. Grid Side Converter Control

For the grid side converter (GSC) in Fig. 6, the reference signals for the DC-link voltage and the reactive power of the grid side converter are passed through two PI controllers. The reference signals are then transformed from dq to abc through the stator angle theta. The generated reference signals $*I_{gabc}$ are then compared to the measured stator currents $I_{g\ (abc)}$. The effective signals are then passed through a second PI, before comparing with a carrier signal to generate

the reference switching signals for the IGBTs in the GSC.

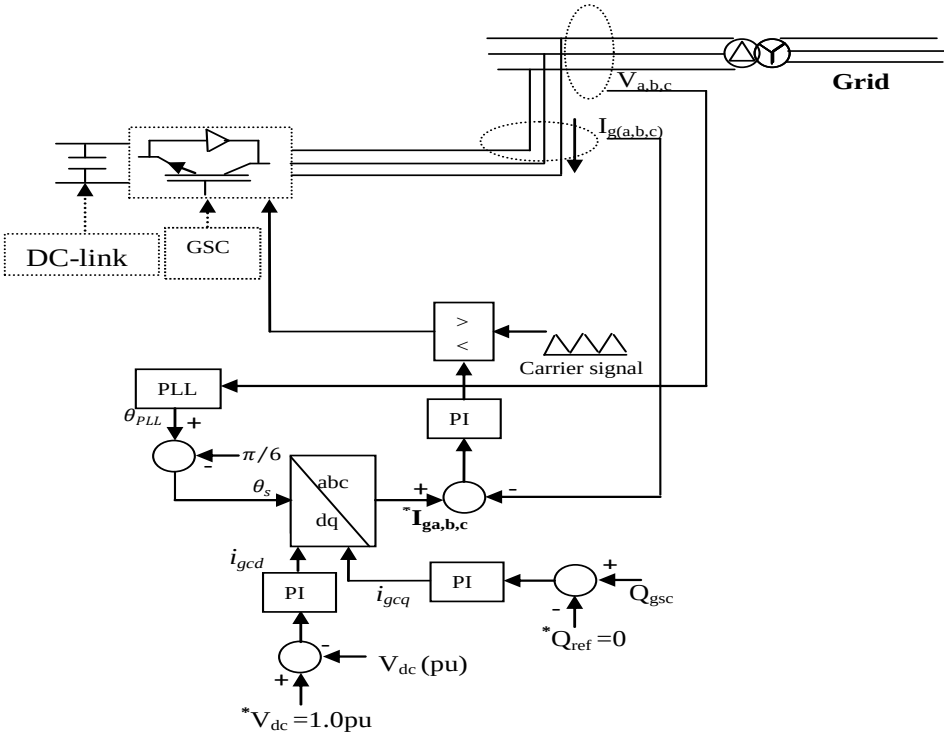

Fig. 6 Block diagram of grid side converter control of DFIG

VII. Simulation Results and Discussion

Simulation analyses were carried out using PSCAD/EMTDC for four cases. In the first case, the DFIGs were replaced by IGs in the wind farms in Fig.1, which will be referred to "no control". In the second case, the VC-VSC based scheme (Scheme 1) is considered to control the DFIG. In the third case, the VC-VSC based scheme with the SDBR (Scheme 2), in which 0.05pu resistance is used, is considered. The proposed CC-VSC based DFIG control scheme (Scheme 3) is considered in the fourth case. Simulations for a three line to ground fault (3LG) at fault point F2 in Fig. 1 have been performed, in which, the fault occurs at 100ms, the circuit breakers on the faulted lines are opened at 200ms, and finally the circuit breakers are re-closed at 1000ms. It is

assumed all the wind turbine generators are operating under the rated wind speed. Responses of the some of network variables and the wind generators are shown in Figs. 7a-7j.

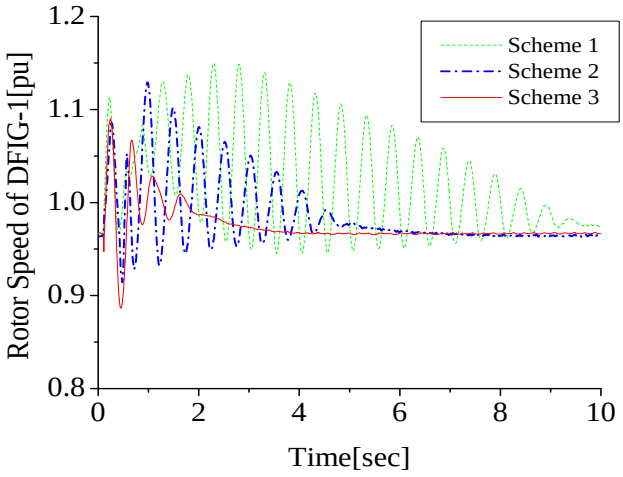

Fig. 7a Rotor speed of DFIG-1

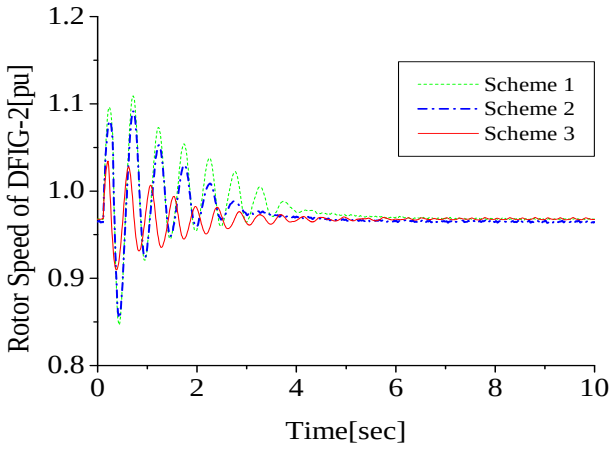

Fig. 7b Rotor speed of DFIG-2

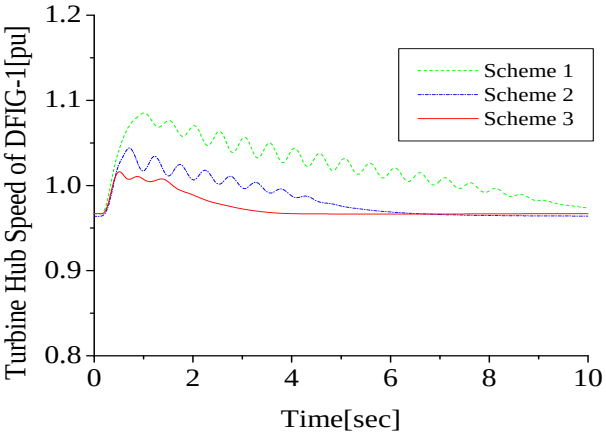

Fig. 7c Wind turbine hub speed of DFIG-1

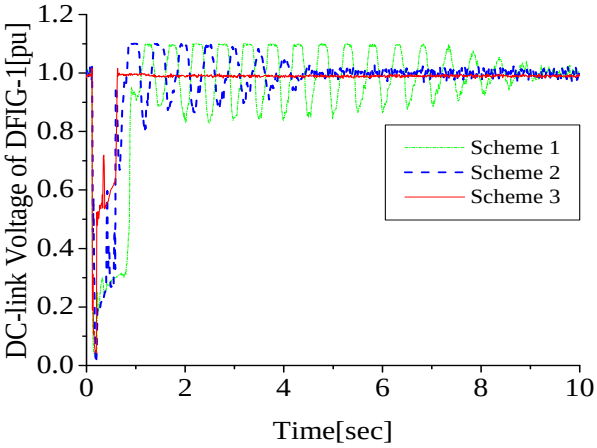

Fig. 7d DC-link voltage of DFIG-1

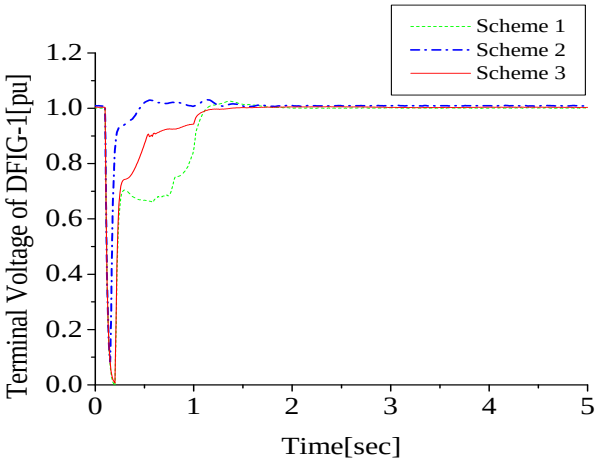

Fig. 7e Terminal voltage of DFIG-1

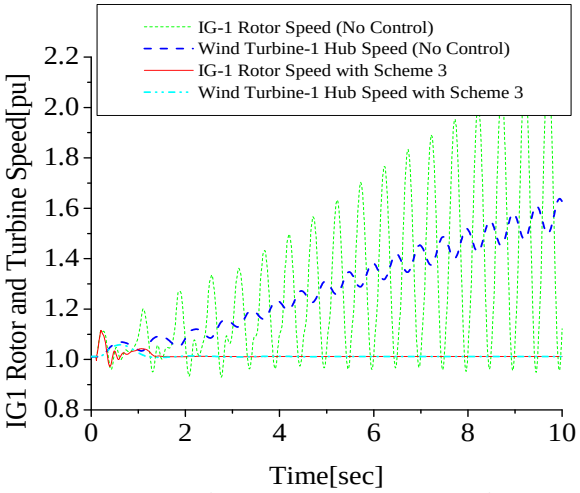

Fig. 7f Rotor and turbine hub speeds of IG-1

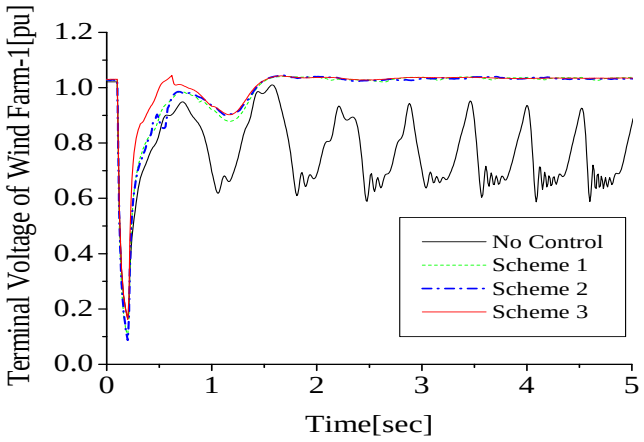

Fig. 7g Terminal voltage of wind farm-1

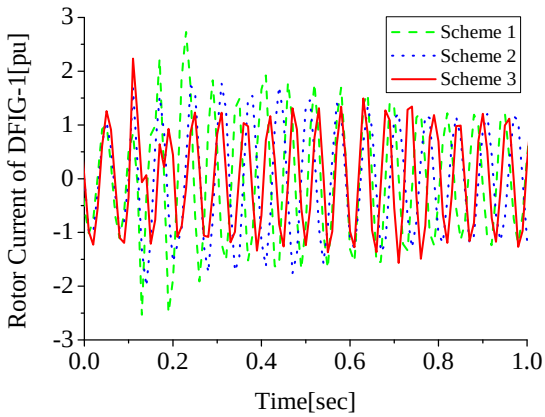

Fig. 7h Rotor current of DFIG-1

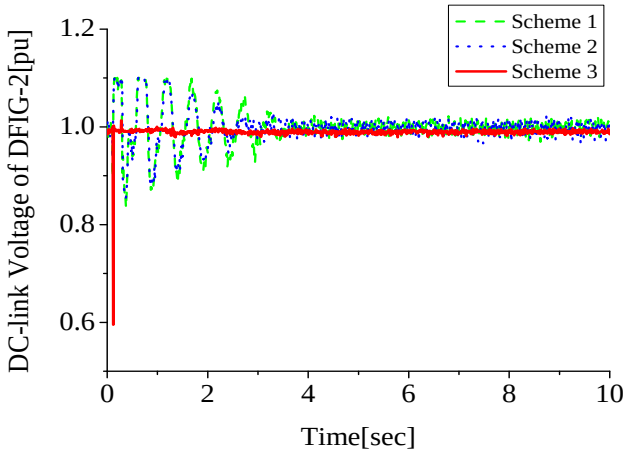

Fig. 7i DC-link voltage of DFIG-2

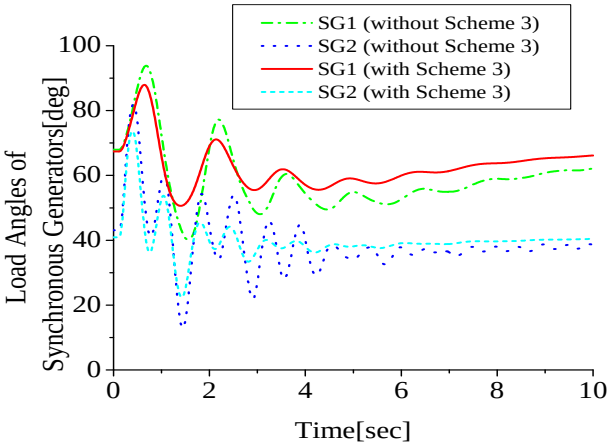

Fig. 7j Load angles of synchronous generators

Figure 7a shows the rotor speed of DFIG-1 in wind farm-1 which is close to fault point F2. It is seen from the figure the rotor speed of DFIG-1 can return to the steady state finally in all of the three schemes. However, scheme 3 gives a better performance with less oscillation compared to schemes 1 and 2. The response of DFIG-2 rotor speed in wind farm-2 is shown in Fig. 7b. The effect of the fault on DFIG-2 rotor speed is small in all schemes because wind farm-2 is far from fault point F2. Scheme 3 gives also in this case better performance than those of schemes 1 and 2. The wind turbine hub speed of DFIG-1 is shown in Fig. 7c, where better response can be achieved in scheme 3.

The DC-link voltage of the DFIG-1 is shown in Fig. 7d. The DC-link voltage can be stabilized in scheme 3, while oscillating responses appear in schemes 1 and 2. This is because scheme 3 can effectively control the DC-link voltage of the DFIG during grid fault. Hence, the DC-link protective device can be omitted in scheme 3.

Figure 7e shows the terminal voltage of DFIG-1. Though it is seen that scheme 2 give a better performance compared to schemes 1 and 3, scheme 2 can give a good performance only in the DFIG terminal voltage. Scheme 3 gives better response of the entire wind farm-1 terminal voltage than other schemes as shown in Fig. 7g, considering grid requirement in Fig. 8. On the other hand, it is also seen from Fig. 7g that, in the case "No Control", in which there is no DFIG control, voltage drop occurs at wind farm-1 and also wind generator terminals. Then, the electromagnetic torques of the IGs drop also as the electromagnetic torque is proportional to the square of the terminal voltage. The mechanical torques of the wind turbines do not change rapidly during the short time interval. As a result, the turbine hubs and generator rotors accelerate due to the large difference between the mechanical and electromagnetic torques, and then, the wind generators become unstable as shown in Fig. 7f. But if any of the DFIG control is applied, the necessary reactive power is supplied, and then, the terminal voltage of the wind farm and the electromagnetic torques of the IGs can be restored quickly and all of the wind generators become stable.

The effectiveness of the rotor current control in DFIG-1 for a 3LG fault for all schemes as shown in Fig. 7h is summarized in Table 4.

Table 4 Effectiveness of DFIG-1 rotor current control for all schemes

Scheme 1	Scheme 2	Scheme 3
The rotor current goes to almost 3 times its nominal value during the grid fault as shown in Fig. 7h.	Though the rotor current was controlled within twice of its nominal value during the grid fault, but much oscillations still occur as shown in Fig. 7h	The rotor current was effectively controlled within twice its nominal value with fewer oscillations during the grid fault as shown in Fig. 7h.

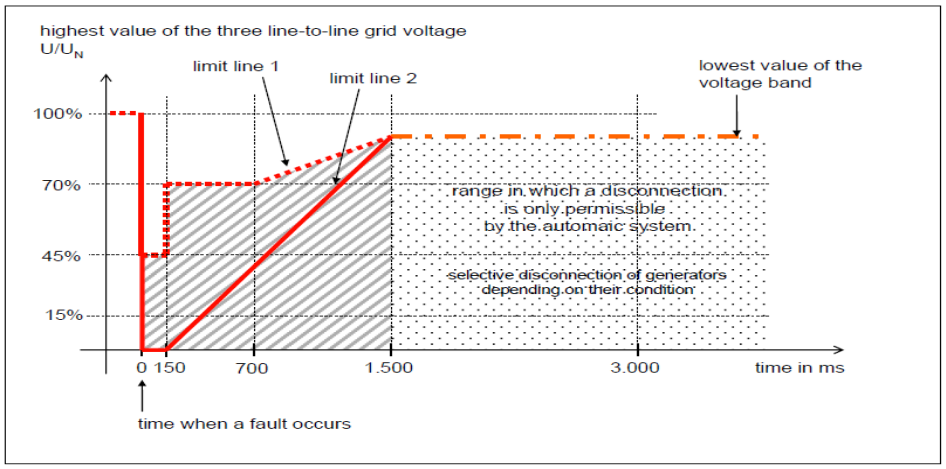

Fig. 8 Fault ride through requirement for wind farm

The response of DFIG-2 DC-link voltage for the 3LG fault which is a severe case that was considered in this study to show the effectiveness of the proposed controller is shown in Fig. 7i. The excessive DC-link voltage excursion observed in DFIG-1 shown in Fig. 7d is due to the fact that the fault occurs close to wind farm 1. The impact of the fault on DFIG-2 DC-link is less because wind farm 2 is far from the fault point. From Figs. 7d and 7i, it is seen that the overvoltage in the DC-link voltage during grid fault, can be reduced significantly using schemes 1 and 2 with the help of DC-link protective device. It is also found that DC-link protection scheme can even be completely omitted when the proposed CC-VSC based control is adopted. Moreover, the DC-link voltages for DFIG-1 and DFIG-2 were able to recover faster with less oscillations after the grid fault for scheme 3 than the other schemes, because of the control strategy employed.

The responses of the load angles of synchronous generators 1 and 2 are shown in Fig. 7j. When the proposed DFIG-based CC-VSC scheme was used, better performance was observed for the load angles of the synchronous generators, showing that the proposed scheme 3, can also enhance the transient stability of synchronous generators connected in the power system.

VIII. Transient Stability Evaluation of the System

The stability index, Wc, [25] defined as follows is used in evaluating the transient stability of the system: $W(\text{sec}) = \int_0^T abs(\frac{d}{dt}W_{total})dt \Big/ system\ base\ power$ (21)

Where T is the simulation time (10.0sec in this case) and W_{total} is the total kinetic energy calculated by using the rotor speed of each synchronous generator as follows:

$$W_{total} = \sum_{i=1}^{N} W_i(J) \tag{22}$$

$$W_i = \frac{1}{2} J_i \omega_{mi}^2(J) \tag{23}$$

Where N is the number of synchronous generators, and J_i and ω_i denote inertia moment and rotor speed of each synchronous generator. The smaller the value of W_c, the better the system transient stability. The transient stability index calculated against one line to ground, two-line to line, two-line to ground and three-line to ground (1LG, 2LS, 2LG, and 3LG) faults at three fault points (F1, F2 and F3 in the model system) with and without considering the proposed scheme 3 are shown in Table 5. From these results it can be understood that the transient stability of the entire power system can be improved by the proposed DFIG control under scheme 3.

Table 5 Transient stability index of the system

	Without DFIG			With DFIG under Scheme 3		
Fault	Fault Location			Fault Location		
	F1	F2	F3	F1	F2	F3
3LG	4.86	3.98	4.62	3.39	2.50	3.11
2LG	3.42	2.32	3.34	2.88	1.64	2.49
2LS	2.98	2.31	2.81	2.41	1.65	2.07
1LG	2.23	1.66	2.22	1.78	1.19	1.56

IX. Optimum Power Capacity of DFIG and IG

Simulation analyses were also carried out to determine the possible largest installation of IG without losing stability taking the wind farm grid code into consideration. A simple model system used in this analysis is shown in Fig. 9. The power capacity of the DFIG was kept constant in all cases and the IG capacity was then gradually increased by 5MW from 30MW to 45MW as shown in Table 6.

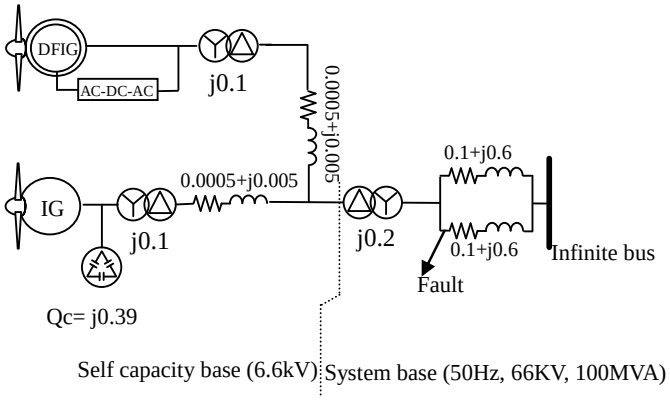

Fig. 9 Simple model system of DFIG and IG

The simulation results show that when the IG capacity is larger than that of DFIG by 10MW (1.5 times larger), the grid voltage can recover within the stipulated 1.5sec set by the grid code as shown in Fig. 10. As the capacity of IG increases over 35MW, the grid voltage takes longer time to be stable (over 1.5 sec) or becomes unstable, and hence the grid code cannot be satisfied in these conditions, as shown also, for example, in Fig.11. Therefore it is concluded that the proposed DFIG controlled under scheme 3 can stabilize IG with the capacity 1.5 times larger with satisfying the grid code in any of fault conditions.

Table 6 Considered cases for possible largest IG capacity

Generators		Results			
DFIG(MW)	IG(MW)	3LG	2LG	L-L	1LG
20	30	O (Fig.10)	O	O	O
20	35	X (Fig.11)	*	*	O
20	40	X	X	X	*
20	45	X	X	X	X

Legend:
O -Stable
* -Does not satisfy the grid code
X- Unstable

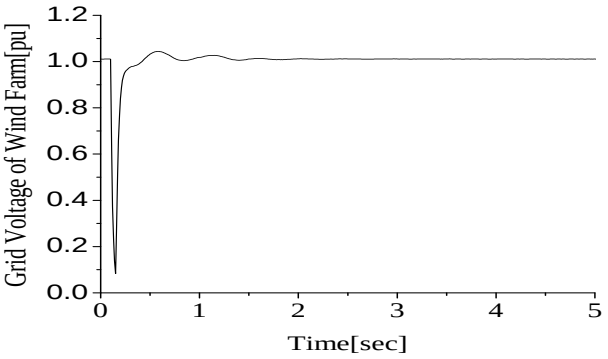

Fig. 10 Grid voltage of wind farm (3LG) (O)

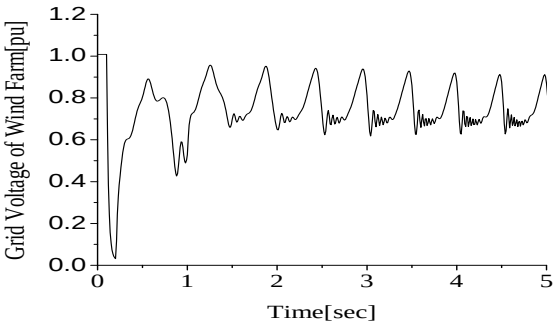

Fig. 11 Grid voltage of wind farm (3LG) (X)

X. Conclusion

This study proposed a new current controlled voltage source converter (CC-VSC) based doubly fed induction generator (DFIG) control scheme. A comparative study using the proposed CC-VSC control schemes and voltage controlled voltage source converter with an SDBR control strategy was presented. The schemes were developed to stabilize wind farms composed of DFIGs and IGs that is connected to a multi-machine power system.

The simulation analyses show that the schemes could effectively control the entire wind farm. However, the proposed CC-VSC scheme is superior to the other schemes considered because of the following reasons. In terms of structure, the dq to abc transformation is only once in the CC-VSC but twice in the VC-VSC scheme. Also the other schemes use the DC-link protective device and combination of the DC-link protective device with an SDBR respectively, for protection during grid fault. These protective devices could be completely avoided in the CC-VSC scheme, leading to less components and switching circuitry, thus the cost and intricacies of the controller design are reduced in the CC-VSC scheme.

Hence, the proposed CC-VSC based DFIG control scheme is recommended because apart from the above mentioned merits, better performance of the DFIGs and the entire wind farms

was achieved during grid fault using the scheme.

Acknowledgement

The authors would like to acknowledge The Petroleum Institute Abu Dhabi, UAE and Japan Gas Corporation for sponsoring this work.

References

[1] Boukhezzar B., and Siguerdidjane H. "Nonlinear control with wind estimation of a DFIG variable speed wind turbine for power capture optimization," Energy Conversion and Management, vol. 50, pp. 885-892, 2009.

[2] Karim-Davijani H., Sheikjoleslami A., Livani H., and Karimi-Davijani M., "Fuzzy logic control of doubly fed induction generator wind turbine," World Applied Science Journal, vol. 6, no. 4, pp. 499-508, 2009.

[3] Manwell J. F., McGowan J., Rogers A., Wind energy explained: thoery design and applications, John Wiley & Sons; 2002.

[4] Bianchi F. D., Battista H. D., Mantz R. J., Wind turbine control systems: principles modeling and gain scheduling design, 2nd ed., Springer: 2006.

[5] Burton T., Sharpe D., Jenkins N., and Bossanyi E., Wind energy handbook. John Wiley & Sons; 2001.

[6] Salles M. B. C., Hameyer K., Cardoso J. R., Grilo A. P., and Rahmann C., "Crowbar system in doubly fed induction wind generators," Energies Journal, vol. 3, pp. 738-753, 2010.

[7] Lindholm M., "Doubly fed drives for variable speed wind turbines," Ph.D Thesis, Technical University of Denmark, 2004.

[8] Holdsworth L., Wu X. G., Ekanayake J. B and Jenkins N., "Comparison of fixed speed and doubly fed induction wind turbines during system disturbnaces," IEEE Proc. Generation Transmission and Distribution 150(3), pp. 343-352, 2007.

[9] Muyeen S. M., Al-Durra A., and Tamura J., "Variable speed wind turbine generator system with current controlled voltage source inverter," Energy Conversion and Management, vol. 52, pp. 2688-2694, 2011.

[10] Muyeen S. M., Ali M. H, Takahashi R., Murata T., Tamura J., Tomaki Y., Sakahara A., and Sasano E., "Comparative study on transient stability analysis of wind turbine generator system using different drive train," IET Renewable Power Generation, 2, vol. 1, no. 2, pp.131-141, 2007.

[11] "*PSCAD/EMTDC Manual*", Manitoba HVDC research center, 1994.

[12] Okedu K. E., Muyeen S. M., Takahashi R., and Tamura J., "Stabilization of wind farms by DFIG-based variable speed wind generators," *International Conference of Electrical Machines and Systems (ICEMS)*, Seoul, South Korea, 2010, available online IEEE Explorer.

[13] Working Group on Prime Mover and Energy Supply Models for System Dynamic Performance Studies, "Hydraulic turbine and turbine control models for fossil fueled steam units on power system studies," IEEE Trans. Power System, vol. 6, no. 2, pp. 753-761, 1991.

[14] Working Group on Prime Mover and Energy Supply Models for System Dynamic Performance Studies, "Hydraulic turbines and turbine control models for system dynamic studies," IEEE Trans. Power System, vol. 7, no. 1, pp. 167-179. 1991.

[15] "*IEEE Recommended Practice for Excitation System Models for Power System Stability Studies*," IEEE STD, 421.5, 1992.

[16] P. Vas, *Sensorless vector and direct torque control*, Oxford University Press, 1995.

[17] Yamamoto M., and Motoyoshi O., "Active and reactive power control for doubly fed wound rotor induction generator," IEEE Trans. Power Electronics, vol. 6, no. 4, pp. 624-629, October, 1991.

[18] S. M. Muyeen, M. H. Ali, R. Takahashi, T. Murata, J. Tamura "Damping of blade-shaft torsional oscillations of wind turbine generator system," Electrical Power Component and Systems Taylor and Francis, vol. 36, no. 2, pp. 195-211, February, 2008.

[19] T. Ghennam, E. M. Berkouk, B. Francois, "Modeling and control of a doubly fed induction generator (DFIG) based wind conversion system," IEEE Trans. On Energy Conversion, pp. 507-512, 2008.

[20] S. Chondrogiannis, M. Barnes, "Stability of doubly fed induction generator under stator voltage oriented vector control," IET Renewable Power and Generation, vol. 2, no. 3, pp. 170-180, 2008.

[21] Okedu K. E., Muyeen S. M., Takahashi R., and Tamura J., "Improvement of fault ride through capability of wind farm using DFIG considering SDBR," European Conference of Power Electronics EPE, Birmingham, United Kingdom, August, 2011, paper number 0306.

[22] Okedu K. E, Muyeen S. M, Takahashi R., and Tamura J., "Application of SDBR with DFIG to Augment Wind Farm Fault Ride Through", ICEMS (International Conference on Electrical Machines and Systems), Beijing, China, August 2011, paper number 026.

[23] Yang J., Fletcher E., and O'Reilly J., "A series dynamic resistor based converter protection schemes for doubly fed induction generator during various fault conditions," IEEE Tran. Energy Convers. Vol. 25, no. 2, pp. 422-432, June, 2010.

[24] Causebrook A., Atkinson D. J., and Jack A. G., "Fault ride through of large wind farms using series dynamic braking resistors," IEEE Trans. Power Systems, vol. 22, no. 3, pp. 966-975, March, 2007.

[25] Yagami M., Shibata S., Murata T. and Tamura J., "An analysis of superconducting fault current limiter for stabilization of synchronous generator in multi-machine system: A two-machine infinite bus system," IEEJ Trans. PE, vol. 123, no. 2, pp. 133-142, 2003.

List of symbols

r_a , X_a	armature resistance and reactance
X_d , X_q	direct and quadrature axes synchronous reactance
$X_d^{/}, X_q^{/}$	direct and quadrature axes transient reactance
$X_d^{//}, X_q^{//}$	direct and quadrature axes subtransient reactance
$T_{do}^{/}, T_{qo}^{/}$	direct and quadrature axes open circuit transient time constant
$T_{do}^{//}, T_{qo}^{//}$	direct and quadrature axes open circuit subtransient time constant
r_1	stator resistance
x_1	stator unsaturated leakage reactance
X_{mu}	unsaturated magnetizing reactance
r_{21}	first cage resistance
x_{21}	rotor unsaturated mutual reactance
r_{22}	second cage unsaturated reactance
SG	synchronous generator
IG	induction generator